

ON THE DEPENDENCE OF THE Q-VALUE ON THE ACCELERATING GRADIENT FOR SUPERCONDUCTING CAVITIES

W. Weingarten, CERN, Geneva, Switzerland[#]

Abstract

The performance of niobium superconducting cavities for accelerator applications has improved considerably over the last decade. Individual cavities reach accelerating gradients close to the theoretical limit (about 50 MV/m), however sometimes at the expense of a re-treatment (baking, electro-polishing, rinsing) needed to eliminate an undesired decrease of the Q-value with the field gradient (Q-slope, Q-drop). Cures have been developed, but a generally accepted physical explanation is still missing. Furthermore, for successful research work on materials other than niobium, it is of utmost importance to understand better the limitations in gradient and Q-value of superconducting cavities. The paper presents an alternative explanation for the Q-slope and confronts it with experimental results for 352 and 1500 MHz cavities.

INTRODUCTION AND SCOPE

The technology of superconducting niobium cavities for accelerator application has made large progress in the last decade. Accelerating gradients between 5 and 10 MV/m that were safely obtained in the past, as for example in the Large Electron Positron collider LEP [1], are now reproducibly surpassed in individual cavities as well as in prototype cryo-modules such as needed for the XFEL at DESY (23.6 MV/m) or the International Linear Collider ILC under design study right now (31.5 MV/m).

This paper is intended to revise earlier and recent experimental results on the decrease of the Q-value with the RF field amplitude, often observed for superconducting accelerating cavities.

Although this decrease is observed as well in niobium cavities manufactured from sheet metal [2], the focus of the paper is directed to niobium film cavities pioneered by CERN for the LEP electron positron collider and now also installed in the Large Hadron Collider LHC. Nevertheless the attempt is made to assess these two technologies (sheet metal and film) under a common viewpoint.

In fact there are three different regimes where the Q-value depends on the accelerating gradient or, equivalently, the maximum applied magnetic surface field amplitude B . In the low field region ($B < 20$ mT) the Q-value may increase with B (low field Q-increase). In the intermediate field region (20-120 mT) the Q-value decreases, and beyond, incidentally, the Q-value may drop even faster. These latter two observations are named "Q-slope" and "Q-drop".

To understand the physical mechanism behind these observations is not only of academic interest, especially

for film cavities. As the reason is neither clear nor mastered, film cavities are disregarded from being a serious competitor to sheet metal cavities. Nonetheless, the many assets of the film technology make it a very serious candidate for large new projects. They include: a better thermal protection against quenches; a lower niobium cost; no need for niobium chemistry; revamping possibility.

POSTULATES

The postulates of the model presented in this paper are the following:

(i) Niobium metal, whether produced as a film or from sheet metal, is inhomogeneous and consists of different composites, say two of them for reasons of convenience. The first, filling up the smaller volume of both, is made up of a weak superconductor with a smaller lower critical field B_0 than that of pure Nb, called "defects". They have a surface density n_{s0} and a size a much smaller than all characteristic lengths of the superconductor (such as the coherence length ξ and penetration depth λ). The second, filling up the larger volume of both, consists of niobium metal, called "bulk", characterized by a lower critical field B_{c1}^* , different from that of ordinary niobium, and a coherence lengths ξ determined by the mean free paths l and the coherence length ξ_0 in the clean limit,

$$\frac{1}{\xi} = \frac{1}{l} + \frac{1}{\xi_0} \quad (1)$$

(ii) The RF losses are created by the transition of these defects from the superconducting to the normal conducting state, starting from B_0 , and increasing the size of its normal conducting volume with increasing magnetic field B . They perform the transition back again into the superconducting state when B decreases again later during the RF cycle. Their inherent condensation energy is dissipated to the helium bath, twice per RF cycle.

THE RF LOSSES ASSOCIATED WITH THE Q-SLOPE

The phase transition as described before is supposed be of second order, because niobium is a type II superconductor, already when being in elemental form and the more when containing impurities. A rigorous approach should therefore be based on the Ginzburg-Landau theory, which, for small ξ , is approximated by the London theory. The latter approach is chosen as a more qualitative approach, the aim being mainly to present for

[#] wolfgang.weingarten@cern.ch

discussion in this workshop a possible explanation for the Q-slope and Q-drop.

The normal-superconducting interface

We imagine an interface between a vacuum or normal conducting metal and a superconducting metal (Fig. 1). The critical magnetic field B_{cl}^* is determined from the fact that the interface energy of type II superconductors becomes negative, if $B > B_{cl}^*$.

In a type II superconductor, characterized by a Ginzburg-Landau parameter $\kappa = \lambda/\xi > 1/\sqrt{2}$, when passing the interface along the z -axis, the condensation into Cooper pairs of the normal conducting electrons reaches its bulk value only after a distance ξ , the coherence length. Likewise, the complete suppression of the magnetic field inside the superconductor only happens at a still further distance λ , the penetration depth. This first effect gives rise to an increase of the condensation energy density $\Delta E_c = 1/(2\mu_0)B_{th}^2 \cdot V_c$ over a volume $V_c = A \cdot \xi$ (surface area A) compared to a situation where the Cooper pair density will reach its bulk value already at the interface $z = 0$. V_c is called the “condensation” volume. B_{th} is the local thermodynamic critical field in the vicinity of the defect that depends on the temperature T as:

$$B_{th}(T) = B_{th0} \cdot \left(1 - \left(\frac{T}{T_c}\right)^2\right),$$

with T_c being the critical temperature.

The second effect gives rise to a decrease of the diamagnetic energy $\Delta E_B = 1/(2\mu_0)B^2 \cdot V_m$ over a volume $V_m = A \cdot \lambda$ compared to a situation where the magnetic field will reach its bulk value already at the interface $z = 0$. B is the externally applied magnetic field. V_m is called the “magnetic” volume. Therefore, when figuring out the energy balance, in a type II superconductor, for sufficiently large B , the diamagnetic energy loss exceeds the condensation energy gain and is therefore energetically favoured. In other words, the interface energy $\Delta E_c - \Delta E_B$ becomes negative. Hence the tendency to create as many interfaces between the normal metal and the superconductor, as is physically possible from an energy and stability point of view. That is the reason why the magnetic field in a type II superconductor splits up into minuscule filaments.

Based on the preceding arguments, the energy balance ΔE between the condensation energy E_c and the diamagnetic energy E_B , for a defect with volume V_c , exposed to a magnetic field B , is

$$\begin{aligned} \Delta E &= \Delta E_c - \Delta E_B = \frac{1}{2\mu_0} \cdot B_{th}^2 \cdot V_c - \frac{1}{2\mu_0} \cdot B^2 \cdot V_m \leq 0 \\ \Rightarrow B^2 \cdot V_m &\geq B_{th}^2 \cdot V_c \end{aligned}$$

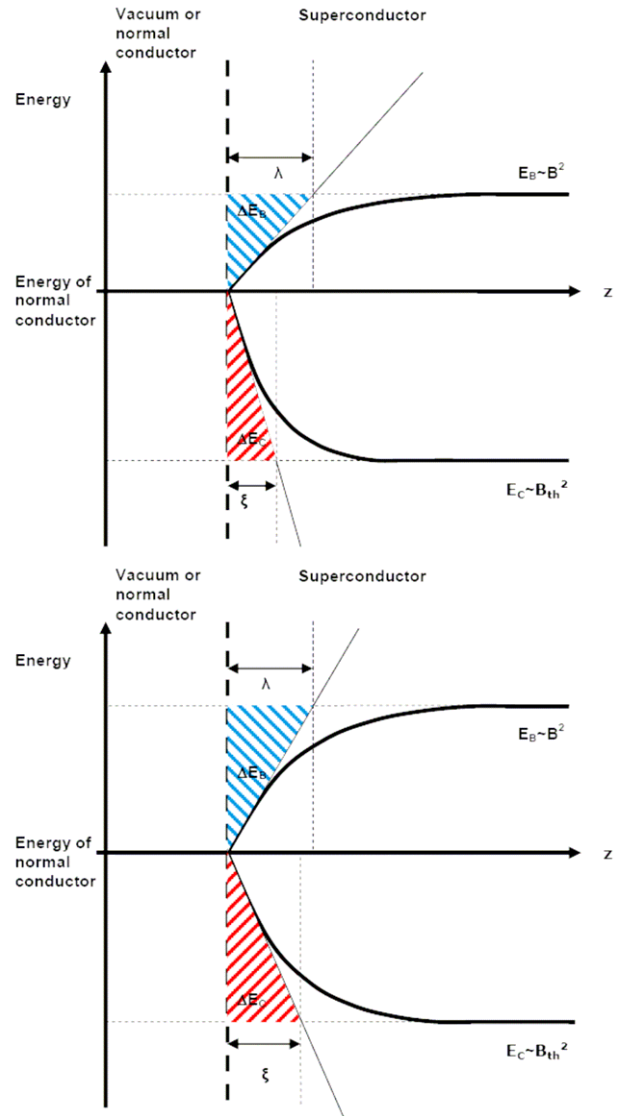


Figure 1: Interface between vacuum or normal conducting metal and superconducting metal for a type II superconductor with at the top a smaller applied magnetic field B than at the bottom. The hatched red and blue areas indicate the condensation energy gain or the diamagnetic energy loss near the interface. They are about equal in size indicating that the magnetic field B is just above the threshold field B_{cl}^* necessary to create the interface normal conductor-superconductor, whereas the magnetic field B inside the superconductor is below that threshold. For increasing magnetic field B , the condensation volume, symbolized by ξ , increases as well (bottom).

Hence, the energy balance ΔE becomes negative once the applied magnetic field B exceeds

$$B_{cl}^* = \sqrt{\frac{V_c}{V_m}} \cdot B_{th}$$

which is equivalent with

$$V_c \cdot B_{th}^2 = V_m \cdot B_{cl}^{*2} \quad (2)$$

For the special case of an interface between a normal-conducting half sphere of radius a embedded at the surface of a superconducting metal, the concerned volumes are $V_m = 2/3 \cdot \pi \cdot (a + \lambda)^3$ and $V_c = 2/3 \cdot \pi \cdot (a + \xi)^3$, from which we derive

$$B_{cl}^* \underset{a \rightarrow 0}{\approx} \left(\frac{\xi}{\lambda} \right)^{3/2} \cdot B_{th}$$

Eq. 2 may be interpreted as a functional relation between the applied magnetic field $B = B_{cl}^*$ and the associated condensation volume $V_c(B)$, with B_{th} and V_m being considered as constant.

Fig. 1 depicts the dependence on the magnetic field B of the condensation volume V_c , being proportional to the coherence length ξ . The top of Fig. 1 illustrates the threshold condition $\Delta E = 0$ for a smaller magnetic field B than at the bottom.

Differentiating eq. 2 results in an expression for the increase of the condensation volume $\Delta V_c(B_{cl}^*)$ by the action of the applied magnetic field ΔB_{cl}^* ,

$$\Delta V_c(B_{cl}^*) = \frac{2 \cdot B_{cl}^* \cdot V_m}{B_{th}^2} \cdot \Delta B_{cl}^* \quad (3)$$

If the magnetic volume V_m is not constant, eq. 3 must be modified to

$$\Delta V_c(B_{cl}^*) = \frac{2 \cdot B_{cl}^* \cdot V_m}{B_{th}^2} \cdot \Delta B_{cl}^* + \left(\frac{B_{cl}^*}{B_{th}} \right)^2 \Delta V_m$$

In this case the following relations hold:

$$\frac{\Delta V_m}{\Delta V_c} = \left(\frac{a + \lambda}{a + \xi} \right)^2 \underset{a < \lambda, \xi}{\approx} \left(\frac{\lambda}{\xi} \right)^2 = \kappa^2,$$

and

$$\Delta V_c = \frac{2 \cdot B_{cl}^* \cdot V_m}{B_{th}^2 - \kappa^2 \cdot B_{cl}^{*2}} \cdot \Delta B_{cl}^* \quad (4)$$

A distinction must be made between the situation, when the defect is located at the surface and when it is located in the bulk, but still within a distance of the penetration depth λ away from the surface and hence exposed to the RF current.

If embedded in the bulk, the current passes around the defect on both sides, when becoming normal conducting. In other words, a loop-like microscopic magnetic field is created with the net result of zero change of magnetic induction in the superconductor: the diamagnetic energy remains unchanged, the energy balance ΔE will not

become negative, and hence no transition from the superconducting state to the normal conducting state will occur. This is the reason why the effect as described here will only take place at the surface and not inside the superconductor.

Determination of the Q -slope related RF losses

The basic idea for determining the RF losses consists in the fact that sufficiently small normal conducting “defects” of radius $a < \xi$ are looped around by the RF currents. The radius a may be considered as equivalent to a local coherence length being smaller than the “bulk”-value. The passing of the RF currents around the normal conducting zones is a situation very similar to the DC case. In what follows a precision shall be given on what means “small” and why is it that the RF current flows around these defects when being in the normal state.

Under what conditions does the RF current loop around the defect when being in the normal conducting state?

The idea is - as in the DC case - that the distribution of current is such that it follows a path that minimizes the production of heat. In other words, the distribution of impedances determines the pattern of current flow. In the present situation the relevant impedances are the ohmic resistance R of the defect and the kinetic inductance L of the bulk superconducting metal after having become normal conducting (as shown in Fig. 2).

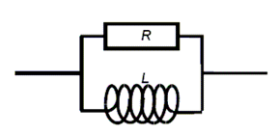


Figure 2: Parallel impedance model description of current with kinetic inductance L looping around a defect with resistance R .

The ohmic resistance amounts to $R = (\sigma \delta)^{-1}$, depending on the conductivity σ and the skin depth δ , whereas the kinetic inductance is $L \sim \mu_0 \cdot a^{2/3} \cdot \lambda^{1/3} / 4$, as shown in the Annex. The condition that the current avoids the normal conducting defect is therefore $\omega \mu_0 \cdot a \leq \omega \mu_0 \cdot a^{2/3} \cdot \lambda^{1/3} \ll (\sigma \delta)^{-1}$. With the normal conducting skin depth, $\delta = (2 / \mu_0 \cdot \sigma \omega)^{1/2}$, the inequality relation implies that the defect size a is small compared to the critical defect size $a_c = \delta^2$. For normal conducting niobium at 1 GHz and 4.2 K, with a room temperature conductivity $\sigma = 7.6 \cdot 10^6$ (Ωm) $^{-1}$, and a residual resistivity ratio $RRR = 10$, the critical defect size is $a_c = 900$ nm. One concludes therefore that the RF current avoids the normal conducting defect if its actual size is much smaller than a_c , say in the order of magnitude of the penetration depth $\lambda \approx 50$ -100 nm or below, very similar to fluxon-induced losses [3].

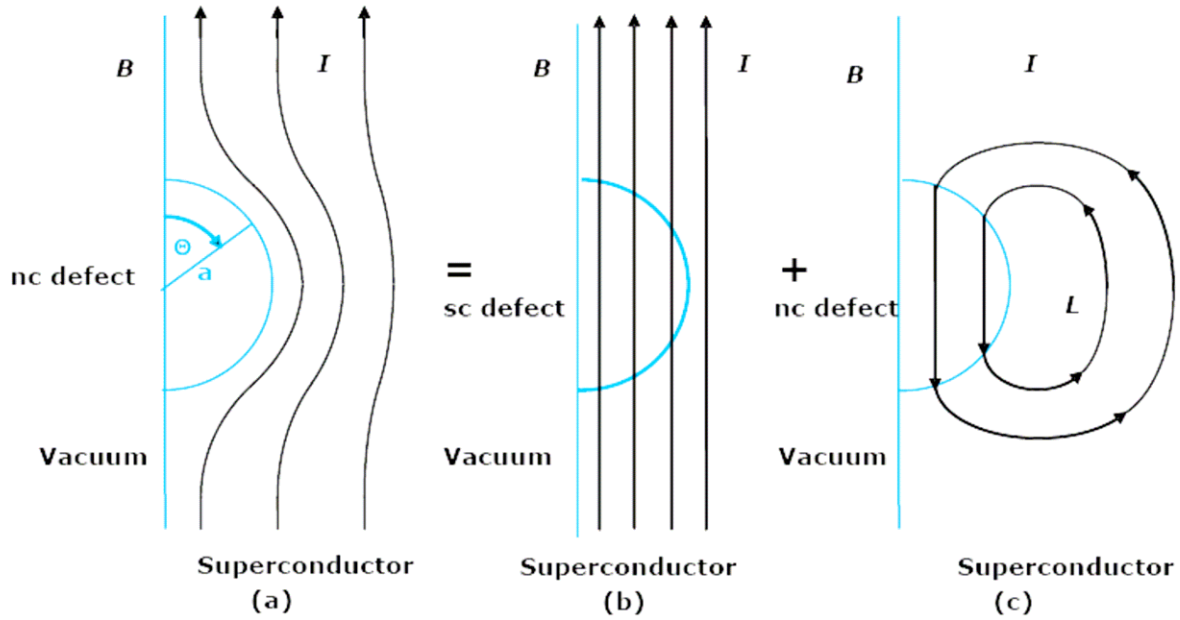


Figure 3: Interface between normal and superconducting metal including a normal conducting “surface defect”; the distribution of current looping around the defect (a) is a superposition of two different current distributions (b, c). Case (b) is equivalent to the defect being in the superconducting state and the current passing through. For case (c) the current inside the defect is opposite to the current in (b), resulting in a net zero current in (a) and giving rise to an additional inductance L , as outlined in the Annex.

DETERMINATION OF THE SURFACE RESISTANCE

Quantitative analysis of the Q -slope

In summary we conclude that, if the defect is located at the surface, upon becoming normal conducting, the RF current loops around it, provided that its radius a is much smaller than the normal conducting skin depth δ . Consequently, when it undergoes the transition from superconducting to normal conducting, a voltage V is created across such that the current I inside the defect vanishes.

The energy balance between the defect being in the superconducting and in the normal conducting state is illustrated in Fig. 3. The energy of the normal conducting state, compared to that of the superconducting state, is increased by three contributions: (i) the condensation energy of the defect, (ii) the kinetic energy of the circulating currents that annihilate the superconducting current through the normal conducting defect, and (iii) the additional magnetic field that these circulating currents create. The second term is not altered by the transition from the superconducting to the normal conducting state, because the current I is supposed to be equal before and after. The third effect does not lead to dissipation, because the induced voltage $V = L \cdot dI/dt$ is in quadrature to the current I . Therefore, only the first effect creates dissipation.

The condensation energy ΔE_c needed to transform the condensation volume ΔV_c normal conducting, is given by the expression

$$\Delta E_c = \frac{1}{2\mu_0} \cdot B_{c1}^{*2} \cdot \Delta V_c$$

Insertion of eq. 3 and integration over B_{c1}^* from 0, for convenience, to the magnetic field amplitude B , results in

$$E_c = \frac{1}{4\mu_0} \cdot B^4 \cdot \frac{V_m}{B_{th}^2}$$

By taking into account that per full RF cycle $T = 1/f$, f being the RF frequency, twice the work ΔE_c will be expended by the RF field, the dissipated power P due to the increase of the normal conducting zone is

$$P = \frac{1}{2\mu_0} \cdot B^4 \cdot \frac{V_m}{B_{th}^2} \cdot f$$

For n_0 defects per volume, the surface density of defects is $n_{s0} = n_0^{2/3}$. Hence the dissipated power p per area is

$$p = \frac{1}{2\mu_0} \cdot B^4 \cdot \frac{V_m}{B_{th}^2} \cdot f \cdot n_{s0}$$

By the definition of the surface resistance R_s , $p = R_s \cdot H^2/2$, $H = B/\mu_0$ being the applied RF magnetic field amplitude, and defining the magnetic volume of a half sphere as $V_m = 2/3 \cdot \pi \cdot \lambda^3$, we derive for the surface resistance

$$R_s = \frac{2}{3} \cdot \pi \cdot \mu_0 \cdot \left(\frac{B}{B_{th}} \right)^2 \cdot \lambda^3 \cdot f \cdot n_{s0} \quad (5)$$

A more refined analysis, by taking into account eq. 4, results in an infinite product expansion

$$R_s = \frac{2}{3} \cdot \pi \cdot \mu_0 \cdot \underbrace{\frac{\lambda^3 \cdot n_{s0}}{B_{th}^2}}_{=\alpha} \cdot f \cdot B^2 \cdot \left(1 + \frac{2}{3} \cdot \underbrace{\left(\frac{\kappa}{B_{th}}\right)^2}_{=\beta} \cdot B^2 \cdot \left(1 + \frac{3}{4} \cdot \underbrace{\left(\frac{\kappa}{B_{th}}\right)^2}_{=\beta} \cdot B^2 \cdot \dots\right)\right),$$

which depends critically, for larger magnetic fields B , on the Ginzburg-Landau parameter κ .

With the two independent fit parameters, $\alpha = \lambda^3 \cdot n_{s0} / B_{th}^2$ and $\beta = (\kappa / B_{th})^2$, which depend via λ , κ , and B_{th} on the temperature T , the surface resistance is

$$R_s(f, B, \alpha, \beta, B_0) = \frac{2}{3} \cdot \pi \cdot \mu_0 \cdot \alpha \cdot f \cdot B^2 \cdot \left(1 + \frac{2}{3} \cdot \beta \cdot B^2 \cdot \left(1 + \frac{3}{4} \cdot \beta \cdot B^2 \cdot \dots\right)\right). \quad (6)$$

The two parameters α and β describe the Q-slope and Q-drop, respectively.

Remarks on the Q-drop

As suggested by the singularity of eq. 4, the surface resistance will grow rapidly above the ‘‘onset’’ magnetic field, if the applied magnetic field $B = B_{c1}^*$ will approach the lower critical field of the bulk $B_{c1} \approx B_{th} / \kappa$.

At that moment, the magnetic volume V_m can no longer be considered as constant, but will increase rapidly with B . The important parameter is the Ginzburg-Landau parameter κ that depends on interstitial impurities such as oxygen. By diffusing these impurities from the surface into the bulk, κ can be decreased with a consequent increase of the onset field for the Q-drop. This mechanism may explain the observed Q-drop as well as the cures that were experimentally found to shift the onset field to higher values [2].

Remarks on the low field Q-increase

The surface resistance as described by eq. 6 needs another modification due to the transition per RF half cycle of the defects, in the very low magnetic field region $B < 20$ mT, into the normal conducting state and back again. In a similar manner as described by eq. 2 the condensation energy

$$E_{c,d} = \frac{1}{2\mu_0} \cdot B_{th,d}^2 \cdot V_{c,d} = \frac{1}{2\mu_0} \cdot B_0^2 \cdot V_m$$

is dissipated, independent of the RF magnetic field amplitude B . The subscript ‘‘d’’ refers to the defect, and B_0 is its critical field. This additional loss results in an additive term for the surface resistance

$$R_{s,d} = \frac{4}{3} \cdot \pi \cdot \mu_0 \cdot \left(\frac{B_0}{B}\right)^2 \cdot \lambda^3 \cdot f \cdot n_{s0}, \quad (7)$$

which explains the low field Q-increase.

EXPERIMENTAL RESULTS

Series RF measurements of 352 and 1500 MHz niobium film cavities

A large number of cavities at 352 MHz and 1500 MHz were tested at CERN, the first series of measurements for validating the specified performance of the niobium film cavities for the LEP collider, the second series for better understanding the behavior of the niobium film under exposure to an RF field. The original papers and the comparison of the results in terms of Q-slope are published elsewhere [4, 5].

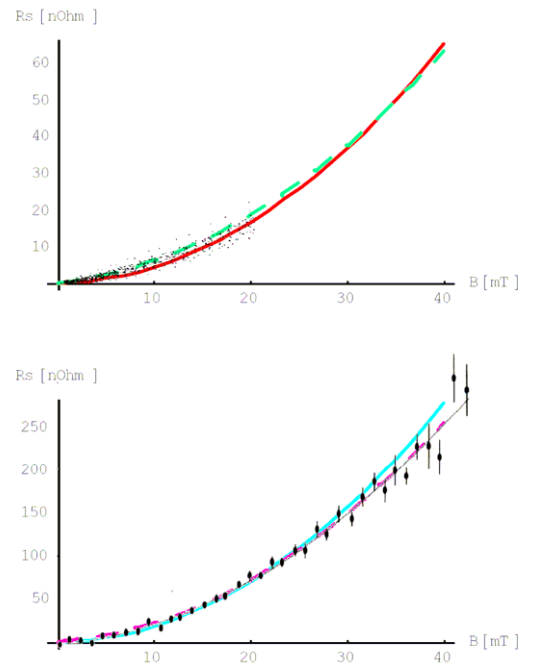


Figure 4: Surface resistance (in $n\Omega$) at 4.2 K of niobium film cavities at 352 MHz (for LEP, top) and 1500 MHz (bottom) versus the RF magnetic field amplitude B (in mT). Superposed in black are the data from the original papers, ref. 4 and 5, respectively. Error bars include the effect of the spread between different films (bottom). The dashed coloured lines indicate the measured values, the continuous coloured ones are calculated by using eq. 5 with, except for the frequency, a common parameter α .

The rationale behind this study was the hope that by analyzing such a large number of cavities (34 at 352 MHz) random variations in RF performance will average out and that the summary data are representative for the physics of the film.

Instead of the Q-slope, the equivalent surface resistance R_s was determined for these two sets of analysis. They are summarized in the relations R_s [n Ω] = 0.26 · B [mT] + 0.033 · B^2 [mT] (4.2 K, 352 MHz) and R_s [n Ω] = 0.741 · B [mT] + 0.140 · B^2 [mT] (4.2 K, 1500 MHz), c.f. Fig. 4.

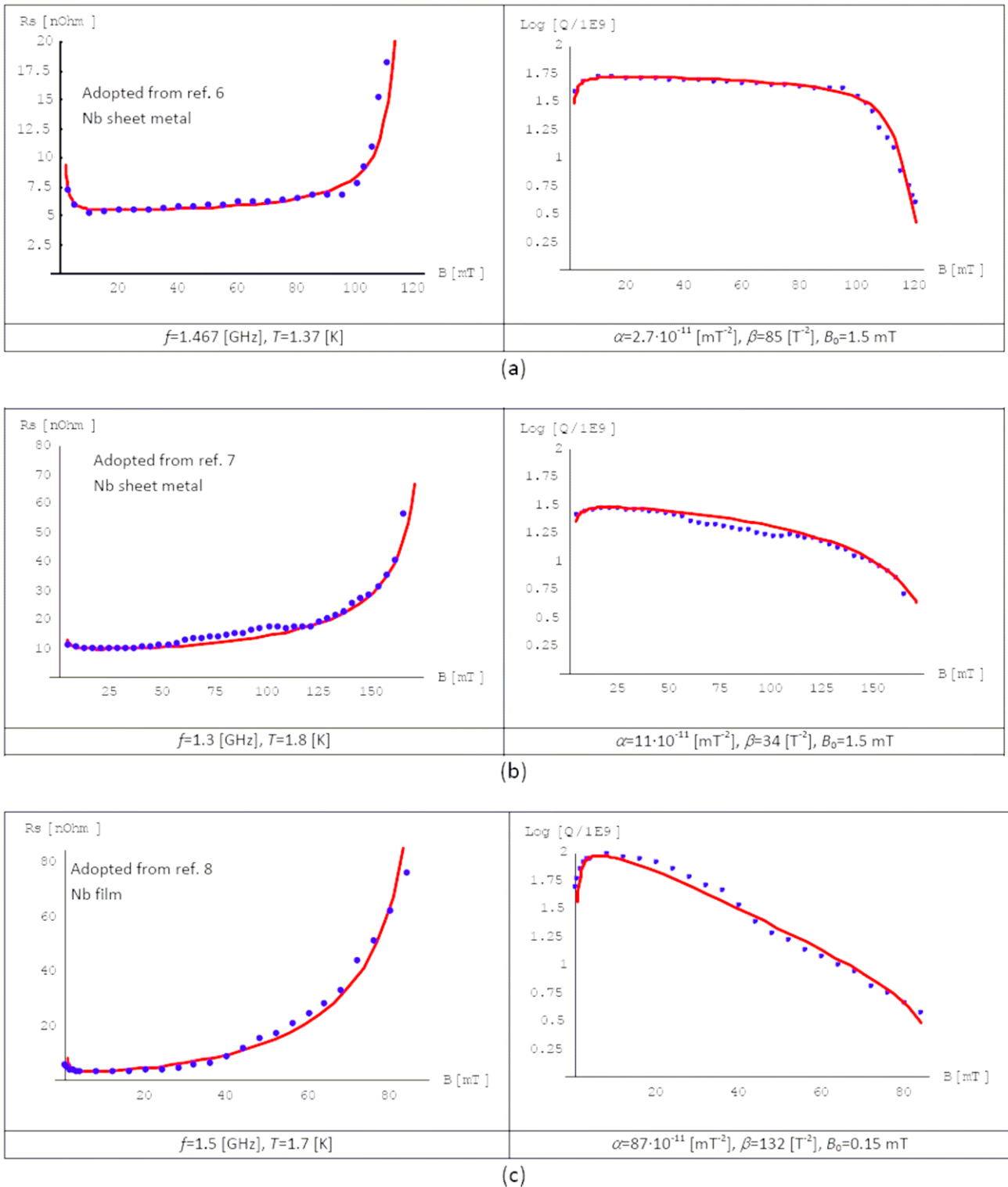


Figure 5: The surface resistance (left column) and the Q -value (right column) of two niobium sheet metal cavities (top) and one niobium film cavity (bottom) displaying the typical low field Q -increase, Q -slope and Q -drop. The fit parameters are indicated in the right column each below the graphs: (a) unbaked; (b) electro-polished and baked; (c) high performance cavity sputtered under Kr gas atmosphere.

The surface resistances R_s determined experimentally are indicated by the dashed coloured lines, those as determined from eq. 5 are represented by the continuous coloured lines. A common set of parameters, the

frequency f excepted, were used to determine R_s from eq. 5 for both sets of data: $\alpha=2.7 \cdot 10^{-8}$ [mT²].

TYPICAL TEST RESULTS OF INDIVIDUAL NIOBIUM SHEET METAL AND FILM CAVITIES

In order to further check the proposed model, some RF tests results of individual sheet metal and film cavities were investigated in more detail. The concerned cavities are representative of state of the art processing. They show the behaviour of Q-slope and Q-drop. The data points were adopted from references 5, 6, and 7 (Fig.5).

The data points were analyzed by applying eq. 6 with the infinite product expansion breaking off after the 25th term and taking into account the term describing the low field Q-increase (eq. 7).

The physical significance of the parameters α and β , as introduced in eq. 6, is the following: α describes the total magnetic volume per unit area (which in fact is a length) prone to undergo the transition from the superconducting to the normal conducting state. This volume is mainly determined by the cube of the penetration depth λ . It remains constant with increasing B until the threshold of the lower critical magnetic field B_{c1} of the bulk is reached. at which moment it increases rapidly. The parameter β is linked to this threshold, being proportional to the square of the Ginzburg-Landau parameter κ .

DATA ANALYSIS

A first and very preliminary example of a possible data analysis shall be presented here, by using the data of Fig. 5 (a) – (c).

No rigorous error analysis is included. The analysis starts with the parameters α and β as well as the penetration depth λ , all three being directly determined by RF measurements.

The analysis is based on well established relations for dirty superconductors [9]. The mean free path l is determined from the relation

$$\lambda(T) = \lambda_L(T) \cdot \sqrt{1 + \frac{\xi_0}{l}}$$

ξ_0 and λ_L are the coherence length and London penetration depth for clean niobium. The coherence length ξ for a dirty superconductor is given by eq. 1.

Using $\kappa = \lambda/\xi$, the thermodynamic critical field B_{th} is determined from $\beta = (\kappa/B_{th})^2$, and the surface density of defects from $\alpha = \lambda^3 \cdot n_{s0}/B_{th}^2$.

It is reassuring that the data analysis (Table 1) results in values for both the thermodynamic critical field B_{th0} and the Ginzburg-Landau parameter κ which are in the range of the expected: $B_{th0} = 186$ (182, 207) mT for $\kappa = 1.7$ (1.0, 2.3) [10].

Assuming the correctness of the model as described, the surface density of defects n_{s0} and the Ginzburg-Landau parameter κ of the film cavity (c) are both much larger than the similar values for the sheet metal cavities (a, b), confirming the larger value of Q-slope that the film cavities display. In addition, the average distance of defects for film cavities $n_{s0}^{-1/2} = 1.2 \mu\text{m}$ lies beyond the

intrinsic lengths such as the grain size, corroborating the possible importance of macroscopic defects relative to the RF performance [8]. The critical field of the defects is much lower (factor $10^2 - 10^3$) than that of the bulk. This information, combined with an analysis of RF tests under different helium bath temperatures, should allow identifying the nature of the defects in the future and hopefully pave the way for their elimination.

Table 1: Preliminary analysis of the data as shown in Fig. 5

	(a)	(b)	(c)
Temperature of helium bath T [K]	1.37	1.8	1.7
Effective penetration depth λ [nm]	36 [6]	30.5 [5]	40 [5]
Fit parameter α [$\text{m}\cdot\text{T}^2$]	$2.7\cdot 10^{-11}$	$11\cdot 10^{-11}$	$87\cdot 10^{-11}$
Fit parameter β [T^{-2}]	85	34	132
Critical field of defect B_0 [mT]	1.5	1.5	0.15
Mean free path l [nm]	61	311	37
Effective coherence length ξ [nm]	21	30	17
Ginzburg-Landau parameter κ	1.7	1.0	2.3
Thermodynamic critical field B_{th0} near defect [mT]	186	182	207
Surface density of defects n_{s0} [m^{-2}]	$2\cdot 10^{10}$	$12\cdot 10^{10}$	$58\cdot 10^{10}$
Clean limit coherence length for Nb $\xi_0 = 33$ nm [5] London penetration depth for Nb $\lambda_L = 29$ nm [5]			

CONCLUSION

The dissipation that becomes manifest by the low field Q-increase, Q-slope and Q-drop is explained in terms of a surface effect caused by the magnetic field.

The superconducting surface is composed of the ordinary superconducting metal (bulk) into which minuscule weak superconducting “defects” are embedded.

These defects lead to dissipation into the helium bath of the condensation energy involved when they undergo the transition, under the action of the RF magnetic field, from the superconducting into the normal conducting state and back again during an RF half cycle.

The dissipation is described in terms of a surface resistance that depends, apart from the experimentally controlled parameters, such as the RF frequency f , bath temperature T and the RF magnetic field amplitude B , on three parameters, B_0 , α and β , describing, in this order, the low field Q-increase, the Q-slope and the Q-drop.

The magnetic field B_0 indicates the critical field of the defect, the parameter α is mainly determined by the density of defects and the cube of the penetration depth λ of the bulk superconductor. The parameter β , is

proportional to the square of the Ginzburg-Landau parameter κ of the bulk superconductor.

A principle way of data analysis was outlined.

The superior performance of state-of-the-art Nb sheet cavities compared to Nb film cavities is explained in terms of a smaller defect density and smaller Ginzburg-Landau parameter.

Evidence is presented for weak superconducting defects (with an average distance beyond the grain size) causing the dependence of the Q-value on the field.

ANNEX: DETERMINATION OF THE INDUCTANCE OF A DEFECT

In the high κ limit, the magnetic induction B outside the weakly superconducting hemispherical defect of radius a is described by the differential equation derived from the London approximation of the Ginzburg-Landau formalism,

$$\frac{1}{\lambda^2} \mathbf{B} + \nabla \times \nabla \times \mathbf{B} = 0$$

which, for spherical coordinates, is identical with

$$-\frac{1}{\lambda^2} (rB_\phi) + \frac{\partial^2}{\partial r^2} (rB_\phi) + \frac{1}{r^2} \frac{\partial}{\partial \Theta} \frac{1}{\sin \Theta} \frac{\partial}{\partial \Theta} (\sin \Theta rB_\phi) = 0$$

$$\frac{1}{\sin \Theta} \frac{\partial}{\partial \Theta} \left(\frac{\sin \Theta}{\sin \Theta} \frac{\partial}{\partial \Theta} rB_\phi \right) - \frac{rB_\phi}{\sin^2 \Theta}$$

Separation of variables by the ansatz

$$B_\phi(r, \Theta) = \frac{u_l(r)}{r} \cdot P_l(\cos \Theta)$$

results in

$$-\frac{1}{\lambda^2} u_l P_l + P_l u_l'' + \frac{u_l}{r^2} \frac{1}{\sin \Theta} \frac{\partial}{\partial \Theta} \left(\sin \Theta \frac{\partial}{\partial \Theta} P_l \right) - \frac{u_l P_l}{r^2 \sin \Theta} = 0$$

$$-\frac{r^2}{\lambda^2} + r^2 \frac{u_l''}{u_l} + \frac{1}{\sin \Theta} \frac{\partial}{\partial \Theta} \left(\frac{\sin \Theta}{P_l} \frac{\partial}{\partial \Theta} P_l \right) - \frac{1}{\sin^2 \Theta} = 0$$

$$\frac{1}{\sin \Theta} \frac{\partial}{\partial \Theta} \left(\frac{\sin \Theta}{P_l} \frac{\partial}{\partial \Theta} P_l \right) - \frac{1}{\sin^2 \Theta} = 0$$

The separation ansatz leads to two differential equations, the first of which is

$$u_l'' - \left(\frac{1}{\lambda^2} + \frac{l(l+1)}{r^2} \right) u_l = 0$$

and

$$\frac{1}{\sin \Theta} \frac{\partial}{\partial \Theta} \left(\sin \Theta \frac{\partial}{\partial \Theta} P_l \right) + \left(l(l+1) - \frac{1}{\sin^2 \Theta} \right) P_l = 0$$

It can be transformed, by means of $u_l(r) = B_\phi \cdot r$, into

$$B_\phi'' - \left(\frac{1}{\lambda^2} + \frac{l(l+1)}{r^2} \right) B_\phi + \frac{2}{r} B_\phi' = 0$$

By finally using

$$B_\phi = \frac{1}{\sqrt{r}} \cdot w_l(r) \quad , \quad x = \frac{r}{\lambda}$$

the equation is identical with the Bessel differential equation [11]

$$x^2 \cdot w_l'' + x \cdot w_l' - \left(x^2 + \left(l + \frac{1}{2} \right)^2 \right) w_l = 0$$

which has the solution that vanishes for $x \rightarrow \infty$,

$$w_l = e^{-x} \cdot \left(\frac{1}{x^{1/2}} + \frac{1}{x^{3/2}} \right)$$

The second differential equation,

$$\frac{1}{\sin \Theta} \frac{\partial}{\partial \Theta} \left(\sin \Theta \frac{\partial}{\partial \Theta} P_l \right) + \left(l(l+1) - \frac{1}{\sin^2 \Theta} \right) P_l = 0$$

transforms, using

$$x = \cos \Theta,$$

into the associated Legendre differential equation

$$(1-x^2)P_l'' - 2xP_l' + \left(l(l+1) - \frac{1}{1-x^2} \right) P_l = 0$$

It is solved by

$$P_l^1(x) = (1-x^2)^{1/2} \frac{d}{dx} P_l(x)$$

Re-inserting back, and taking into account the boundary conditions for $r = a$,

$$B_\phi(\Theta)|_{r=a} = \mu_0 \cdot \frac{H_0 \cdot a \cdot \sin \Theta}{2 \cdot \lambda}$$

one finds for the magnetic induction outside the defect, when $a \leq r$, $a \ll \lambda$, with H_0 the applied magnetic field,

$$B_{\phi,o}(H_0, r, \Theta) = \mu_0 \cdot \frac{H_0}{2} \cdot \left(\frac{a}{\lambda} \right)^3 \cdot \frac{e^{-(r-a)/\lambda}}{\left(\frac{r}{\lambda} \right)^2} \cdot \frac{1 + \frac{r}{\lambda}}{1 + \frac{a}{\lambda}} \cdot \sin \Theta$$

and inside the defect, $r \leq a$,

$$B_{\phi,i}(H_0, r, \Theta) = \mu_0 \cdot \frac{H_0}{2} \cdot \left(\frac{r}{\lambda} \right) \cdot \sin \Theta$$

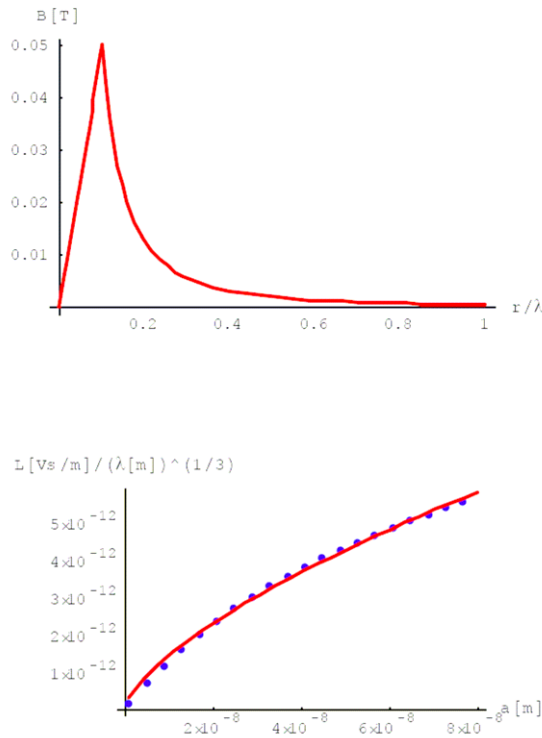


Figure 6: Magnetic induction $B_{\Phi}(r/\lambda)$. The defect size is $0.1 \cdot a$ (top). The inductance L divided by the third root of the penetration depth λ vs. the defect radius a is described by eq. 9 (bottom).

The magnetic induction $B_{\Phi}(r/\lambda)$ is depicted in Fig. 6 in units of Tesla, as calculated for $\Theta = \pi/2$ and $\mu_0 \cdot H_0 = 1$ T.

The stored energy E_B is the sum of the stored energy inside and outside the defect (Fig. 6, top):

$$E_B = \frac{\pi}{2 \cdot \mu_0} \cdot \int_0^{\pi} d\Theta \cdot \sin \Theta \int_0^{\infty} dr \cdot r^2 B_{\Phi,i}^2(H_0, r, \theta) + \frac{\pi}{2 \cdot \mu_0} \cdot \int_0^{\pi} d\Theta \cdot \sin \Theta \int_0^a dr \cdot r^2 B_{\Phi,o}^2(H_0, r, \theta) \quad (8)$$

With the current I passing through the defect, being composed of the product of the current density and the cross section of the defect,

$$I = \frac{B}{\mu_0 \cdot \lambda} \cdot \frac{\pi \cdot a^2}{2},$$

the inductance L is

$$L = \frac{2 \cdot E_B}{I^2}$$

The inductance as calculated point by point by numerical integration of eq. 8 using MATHEMATICA[®] is nicely fitted by the relation (Fig. 6, bottom)

$$L \approx 3.3 \cdot 10^{-7} \cdot a^{2/3} \cdot \lambda^{1/3} \approx \frac{\mu_0}{4} \cdot a^{2/3} \cdot \lambda^{1/3} \quad (9)$$

REFERENCES

- [1] K. Hübner, *Designing and building LEP*, Physics Reports **403 – 404** (2004) 177.
- [2] G. Ciovati, *Review of the frontier workshop and Q-slope result*, Physica C **441** (2006) 44, Proceedings of the 12th International Workshop on RF Superconductivity, Cornell University, Ithaca New York, USA, July 10 – 15, 2005.
- [3] W. Weingarten, *Fluxon-induced losses in niobium thin-film cavities*, Physica C **339** (2000) 231.
- [4] W. Weingarten, *The dependence on the RF frequency of the field dependent part of the surface resistance of niobium sputter coated copper cavities*, Proc. of the 10th Workshop on RF Superconductivity, Tsukuba, Japan, 2001, p. 378.
- [5] C. Benvenuti, S. Calatroni, I. E. Campisi, P. Darriulat; M.A. Peck, R. Russo; A.-M. Valente, *Study of the surface resistance of superconducting niobium films at 1.5 GHz*, Physica C **316** (1999) 153.
- [6] G. Ciovati, *Effect of low-temperature baking on the radio-frequency properties of niobium superconducting cavities for particle accelerators*, Journ. Appl. Phys. **96** (2004) 1591.
- [7] L. Lilje, C. Antoine, C. Benvenuti, D. Bloess, J.-P. Charrier, E. Chiaveri, L. Ferreira, R. Losito, A. Matheisen, H. Preis, D. Proch, D. Reschke, H. Safa, P. Schmüser, D. Trines, B. Visentin, H. Wenninger, *Improved surface treatment of the superconducting TESLA cavities*, Nucl. Instr. Meth. A **516** (2004) 213.
- [8] C. Benvenuti, S. Calatroni, P. Darriulat, M.A. Peck, A.-M. Valente, and C. A. Van't Hof; *Study of the residual resistance of superconducting niobium films at 1.5 GHz*, Physica C **351** (2001) 421.
- [9] e.g. M. Tinkham, *Introduction to Superconductivity*, Malabar, FA, USA, 1980.
- [10] C. C. Koch, J. O. Scarbrough, and D. M. Kroeger, *Effects of interstitial oxygen on the superconductivity of niobium*, Phys. Rev. **B 9** (1974) 888.
- [11] e.g. Jahnke-Emde-Loesch, 7th edition by F. Loesch, *Tables of higher functions*, Stuttgart 1966, p. 207.